This is a post-peer-review, pre-copyedit version of an article published in Climate Dynamics. The final authenticated version is available online at: https://doi.org/10.1007/s00382-019-05048-w

Extratropical cyclones over East Asia: Climatology, seasonal cycle, and long-term trend

Jaeyeon Lee[1], Seok-Woo Son[1]*, Hyeong-Oh Cho[1], Junsu Kim[2], Dong-Hyun Cha[3], John R. Gyakum[4], and Deliang Chen[5]

[1]School of Earth and Environmental Sciences, Seoul National University, Seoul, Republic of Korea

[2]Advanced Modeling Infrastructure Team, Numerical Modeling Center, Seoul, Republic of Korea

[3]School of Urban and Environmental Engineering, Ulsan National Institute of Science and Technology, Ulsan, Republic of Korea

[4]Department of Atmospheric and Oceanic Sciences, McGill University, Montreal, Canada

[5]Regional Climate Group, Department of Earth Sciences, University of Gothenburg, Gothenburg, Sweden

*Corresponding author: Seok-Woo Son, School of Earth and Environmental Sciences, Seoul National University, 1 Gwanak-ro, Gwanak-gu, Seoul, 08826, Republic of Korea. E-mail: seokwooson@snu.ac.kr

This is a post-peer-review, pre-copyedit version of an article published in Climate Dynamics. The final authenticated version is available online at: https://doi.org/10.1007/s00382-019-05048-w

Abstract

Extratropical cyclones (ETCs) in East Asia are automatically detected and tracked by applying a Lagrangian tracking algorithm to the 850-hPa relative vorticity field. The ETC statistics, which are derived from ERA-Interim reanalysis dataset from 1979 to 2017, show that East Asian ETCs primarily form over Mongolia, East China, and the Kuroshio Current region with a maximum frequency of six to seven cyclones per month. Both Mongolia and East China ETCs are initiated on the leeward side of the mountains. While Mongolia ETCs downstream of the Altai–Sayan Mountains develop slowly, East China ETCs downstream of the Tibetan plateau develop rapidly as they travel across the warm ocean. Both of them show a maximum frequency and intensity in spring rather than in winter. In contrast, oceanic ETCs across the Kuroshio Current and the Kuroshio–Oyashio Extension, where sea surface temperature gradient is sharp, reach a maximum frequency in winter although their intensity is still maximum in spring. On the decadal timescale, both ETC frequency and intensity exhibit insignificant trends. Exceptions are springtime East China and summertime Mongolia ETCs whose frequencies have slightly decreased since 1979. This declining trend is consistent with the enhanced static stability in the region.

Keywords: Extratropical cyclone (ETC), East Asia, Lagrangian tracking algorithm, Climatology, Seasonal cycle, Long-term trend

1. Introduction

Climatic features of extratropical cyclones (ETCs) in East Asia have been widely documented in the literature after the pioneering work by Chung et al. (1976). By manually detecting and tracking ETCs in the year 1958, Chung et al. (1976) reported that East Asian ETCs typically develop on the leeward side of major mountain barriers, similar to the development of lee cyclones in the Canadian Rockies. Whittaker and Horn (1984) confirmed this finding by extending the analysis to a more extended period (1958–1977). They found that East Asian ETCs commonly form along the east coast of East China. These oceanic (or coastal) ETCs are generally stronger than continental ETCs. Chen et al. (1991) later updated the work of Whittaker and Horn (1984) by examining daily surface weather maps for the period 1958–1987. The leeward cyclogenesis region downstream of the Altai–Sayan Mountains and the coastal cyclogenesis region over warm ocean water from the East China Sea to the East Sea/Sea of Japan were identified as the main regions of cyclogenesis in their study (see Fig. 1a for the geographical locations of these regions and sea surface temperature (SST)).

The above studies manually detected and tracked ETCs with 12-hourly or daily surface weather maps. This approach is acceptable for studying extreme or well-defined ETCs but might have difficulty in examining weak and relatively small-scale ETCs. To overcome this caveat and to utilize gridded dataset, recent studies have used automated algorithm (see the review by Neu et al. (2013)). It allows for detecting and tracking a large number of ETCs systematically and objectively. The automated algorithm is particularly advantageous for long-term gridded datasets. A series of studies have utilized an automated algorithm to study East Asian ETCs. Adachi and Kimura (2007) constructed the cyclogenesis and ETC track density maps in East Asia by applying the nearest-neighbor method to 6-hourly surface pressure field obtained from a reanalysis data. They reaffirmed the previous findings that active cyclogenesis regions are distributed along the leeward side of mountains and the Kuroshio Current and the Kuroshio-Oyashio Extension (hereafter simply Kuroshio region). By separately examining the merging and splitting of ETCs, Inatsu (2009) found that ETC merging is frequent in the western North Pacific. He reported that the merged ETCs develop more rapidly than other ETCs. Zhang et al. (2012) used the mean sea level pressure (MSLP) field to detect and track ETCs and found that the West Siberian plain, Mongolia, and the coastal regions of East China are major cyclogenesis regions. Chen et al. (2014), who applied a Hodges' algorithm (Hodges et al. 1999) to 6-hourly relative vorticity field, further reported that Mongolia (including the Altai–Sayan Mountains) is a primary source region for East Asian ETCs while East China is a secondary source region.

The factors that determine ETC developments, especially for rapidly developing ETCs which are often referred to as explosive cyclones or meteorological bombs (Sanders and Gyakum 1980), have also been examined. Unlike normal ETCs, explosive ETCs are mainly observed over the East Sea/Sea of Japan and the northwest Pacific near the Kuroshio Current (e.g., Chen et al. 1992). This bimodal distribution in space, with a local minimum over the islands of Japan, is explained by intense heat transport from warm ocean currents around Japan to the atmosphere (e.g., Chen et al. 1992) and enhanced low-level baroclinicity due to a sharp SST gradient (e.g., Yoshida and Asuma 2004).

Most of the aforementioned studies, however, are focused on cyclogenesis and cyclone frequency. Other properties of East Asian ETCs, such as ETC intensity, lysis, developing rate, lifetime and traveling speed, are not well documented. More importantly, the seasonal cycle of East Asian ETCs is not fully understood. Most studies on East Asian ETCs are primarily focused on cold season, although the previous studies on Pacific, Atlantic, and European ETCs have suggested the importance of summertime ETCs (Mesquita et al. 2008; Dong et al. 2013; Gagen et al. 2016) and overall seasonal cycle (Mesquita et al. 2010). Adachi and Kimura (2007), for instance, showed that ETCs that develop from the mouth of the Yangtze River and the East China Sea to the northeastern region of Taiwan have the maximum cyclogenesis in winter. However, Wang et al. (2009) documented that ETCs in Mongolia and northeastern China have a maximum frequency in spring.

It is also unclear whether East Asian ETCs have undergone any long-term changes. Wang et al. (2009) reported that the ETC frequency and intensity were significantly decreased in the 40°–45°N latitude band during the last few decades. Chen et al. (2014) and Cho et al. (2018) also documented a weakening of wintertime ETCs in China and a decreasing number of springtime ETCs in southern China, respectively. In contrast, Iwao et al. (2012) showed that the number of explosive cyclones has slightly increased in the east of Japan. These studies, however, are based either on a relatively small domain (e.g. Mongolia and northeastern China) or just for one season. A comprehensive trend analysis covering East Asia (Fig. 1) and all four seasons has not been conducted with the modern reanalysis data.

The present study aims to extend and update previous studies by documenting more detailed statistics of East Asian ETCs. Analyses are not limited to cyclogenesis and cyclone frequency but conducted for various other ETC properties. Their seasonal cycle and long-term trends are also quantitatively evaluated.

Unlike the previous studies that utilized the MSLP field, the present study identifies ETCs on the 850-hPa relative vorticity field (Hoskins and Hodges 2002). The MSLP field has been traditionally used for ETC detection and tracking. Either the local minimum or its gradient is particularly used to define the center of ETC. Although this approach is successful in capturing a well-organized cyclone, it often misses weak and unorganized cyclones particularly over the complex terrain (Sinclair 1994; Hodges 1999) as in East Asia (Fig. 1). In this regard, the relative vorticity is advantageous because it allows for the early detection of weak and less-organized ETCs (Hoskins and Hodges 2002). The 850-hPa isobaric surface is also practically useful as it minimizes the negative effects of underground extrapolation except over the Tibetan Plateau (Chen et al. 2014).

The paper is organized as follows. Data and methods are described in Section 2. Climatic features, seasonal cycles, and long-term trends of East Asian ETCs are discussed in Section 3. Finally, the summary and discussion are presented in Section 4.

2. Data and methods

ETCs are automatically detected and tracked by applying the algorithm, which was originally developed by Hodges (1994, 1995, 1999), to the 6-hourly relative vorticity field from the European Centre for Medium-Range Forecasts (ECMWF) Re-Analysis interim (ERA-Interim) dataset (Dee at al. 2011) from 1979 to 2017. This algorithm has been evaluated well and applied to various datasets, such as reanalysis data (e.g., Hoskins and Hodges 2002), general circulation model output (e.g., Bengtsson et al. 2006), and regional climate model output (e.g., Côté et al. 2015) for both global and regional ETC studies (Grise et al. 2013; Zappa et al. 2013; Chen et al. 2014; Plante et al. 2015).

To define synoptic scale ETCs, the relative vorticity field is first filtered at a T42 spectral resolution (approximately 2.8° in latitude), which contains the total wavenumbers within a range from 5 to 42. This filtering effectively removes the background flow and small-scale disturbances. A segmentation technique, called as a connected component labeling (Rosenfeld and Kak 1976), is then applied to identify the local maximum of relative vorticity, i.e., the center of ETCs. The connected component labeling is the method of separating the connected grids (occupied by ETC) from the unconnected grids (outside of ETC). In this way, the relative vorticity object can be separated from the background field. The center of ETC, which is defined as a local maximum of the labeled vorticity object, is tracked in the automated algorithm. To get the smoothed trajectory, a cost function, which combines the direction and speed of the moving ETC, is minimized (Hodges 1994, 1995, 1999).

In this study, quasi-stationary thermal lows, which do not intensify with time, are removed by considering ETCs only with a minimum intensity greater than 1.0×10^{-5} s^{-1} (or 1 cyclonic vorticity unit; CVU), a lifetime longer than two days, and a traveling distance greater than 1000 km (Hoskins and Hodges 2002; Grise et al. 2013). Tropical cyclones and their transitions into ETCs are excluded by neglecting all detected cyclones that travel across 25°N from the tropics.

The ETC statistics are computed for frequency, intensity, genesis and lysis locations, growth rate, decay rate, lifetime, speed, and traveling distance. A definition of each property is explained in Table 1. In all cases, ETC statistics are shown in latitude-longitude grids with a 1.5° grid spacing. Here, the statistics at a given grid point represent that of all ETCs passing through within an effective radius of 555 km from the grid point (e.g., Sinclair 1997; Grise et al. 2013). For instance, ETC frequency of one per month at a given grid point implies that the grid point is influenced by at least one ETC, which is located within 555-km from this grid point, per month. As such, the same ETC can be counted at multiple grid points. If the same ETC is counted more than once at a given grid point (this is the case when the ETC is moving slowly), only the first occurrence is considered. Note that this method for ETC statistics is different from the method used in several other studies (e.g., Chung et al. 1976; Chen et al. 1991; Adachi and Kimura 2007) where ETC statistics at a given grid point are analyzed by considering the ETCs passing through a given grid point without considering a radius of influence. Comparing with the classical method, this method makes it possible to analyze the ETCs that may affect the grid point.

3. Results

Figure 1 shows the analysis domain. East Asia is characterized by complex topography with the Tibetan Plateau (~30°N) and the Altai–Sayan Mountains (~45°N) in the west and the open ocean in the east. Over the continent, the thick gray contour denotes the 1.5-km topography. Although it is not shown, this contour approximately corresponds to the line where the surface pressure is 850 hPa. It implies that ETC tracking based on the 850-hPa relative vorticity is not reliable in regions where the topography exceeds approximately 1.5-km altitude.

In the open ocean, SST exhibits a sharp meridional gradient along the Kuroshio–Oyashio Extension (shaded in Fig. 2a). Although it is relatively weak, a strong SST gradient also appears in the East Sea/Sea of Japan. A sharp SST gradient along the Kuroshio-Oyashio extension is related to a strong westerly jet in the upper troposphere through the thermal wind balance (Fig. 2b). Many weather systems developing in East Asia travels eastward along this jet. Here, it is noteworthy that East Asia is located at the entrance region of the jet. In terms of synoptic meteorology, the equatorward side of jet entrance is dominated by ascending motion (Uccellini and Kocin 1987). This may enhance ETC development across East China and possibly enhance lee cyclogenesis downstream of the southern Tibetan Plateau.

Figure 2c illustrates the background Eady growth rate (Lindzen and Farrell 1980; Hoskins and Valdes 1990) that could explain the baroclinic development of local ETCs.

Although this property is based on linear dynamics and is typically applied to zonal-mean flow, it is still useful for understanding developing mid-latitude weather systems. The Eady growth rate, σ, is defined as

$$\sigma = 0.31\, f\, |\partial u/\partial z| N^{-1},$$

where f is the Coriolis parameter (in s^{-1}), u is the zonal wind (in m s^{-1}), and N is the Brunt-Väisälä frequency (in s^{-1}). The zonal wind and the potential temperature at 500- and 850-hPa pressure levels are used to compute σ in the lower troposphere. Although not shown, essentially the same result is also found when 700- and 850-hPa pressure levels are used.

The Eady growth rate is large over the broad region from the central and northern China to the Kuroshio region due to relatively weak static stability over the continent (not shown) and strong vertical wind shear across the Kuroshio region (Fig. 2b). These background conditions may promote lee cyclogenesis around Mongolia and coastal cyclogenesis around the Kuroshio Current (e.g., Chen et al. 1991; Adachi and Kimura 2007; Chen et al. 2014).

By considering these background states, the following subsections describe the climatological characteristics of East Asian ETCs. Their seasonality and long-term trend are also documented.

3.1. Climatology

Climatological features of East Asian ETCs during 1979–2017 are presented in Fig. 3. The first three panels show ETC genesis (Fig. 3a), frequency (Fig. 3b), and intensity (Fig. 3c). The other panels show growth (Fig. 3d), decay rates (Fig. 3e), cyclolysis (Fig. 3f), lifetime (Fig. 3g), traveling speed (Fig. 3h) and distance (Fig. 3i). These properties are shown only at the grid point where ETC frequency is greater than one.

The ETC frequency, as shown in Fig. 3b, is pronounced in west Siberia northern region, lee side of mountains, and near the Kuroshio Current. This is partly consistent with Zhang et al. (2012) who reported that Eurasian ETCs often form over the West Siberian plains, Mongolia, and the coastal regions of East China, then decay in Siberia north of 60°N, northeast China, and the Okhotsk Sea-northwest Pacific region in the MSLP field. The ETC frequency is maximum over the northern region of Western Siberian Plain. Figures 3a and c, however, show that West Siberian ETCs are not strong and only a few ETCs are generated in this region when detected from the 850-hPa relative vorticity field. As discussed in Chen and Zhang (1996), ETCs in this region typically begin to grow on the leeward side of the Ural Mountains and travel eastward. Among them, the ETCs reaching west Siberia north develop rather slowly (Fig. 3d) and travel a long distance towards this region (Fig. 3i) at a relatively fast speed (Fig. 3h), then eventually decay at approximately 80°E (Fig. 3f). Because they are typically decaying systems without noticeable impacts on East Asian weather, the characteristics of these ETCs are not discussed later in this study.

The ETCs that affect East Asian weather typically form on the lee side of the Altai-Sayan Mountains and the Tibetan Plateau as well as over the east coast of Japan (Fig. 3a). These ETCs develop approximately three to six times per month with a local maximum near Mongolia and the Kuroshio region (Fig. 3b). The detected ETCs are relatively strong with mean intensity ranging from two to five CVU, with increasing intensity from the continent to the open ocean (Fig. 3c).

The growth rate of East Asian ETCs is typically larger than 1.6 CVU per day with a distinct maximum over the Kuroshio region (Fig. 3d). Most ETCs decay over the Okhotsk Sea with a maximum decay rate of more than -1.2 CVU per day (Fig. 3e). On average, ETCs are sustained for approximately five days (Fig. 3g) and travel more than 4,000 km in mid-latitudes at a speed of about 40 km per hour (Figs. 3h, i).

Among the three cyclogenesis regions (Fig. 3a), ETCs form most frequently in downstream region of the Altai–Sayan Mountains. These ETCs, which are referred to as Mongolia ETCs in this study (box “A” in Fig. 3b), are not as strong as West Siberia ETCs (Fig. 3c), but they are newly formed cyclones (Fig. 3a) that grow quickly over time (Fig. 3d). Chen and Lazić (1990) showed that Mongolia ETCs are often initiated by a cutoff low. When a mid-tropospheric trough sweeps past the northern region of the Altai-Sayan Mountains, it rapidly develops and turns into a cutoff low within a couple of days. The induced surface cyclones slowly move towards northeast China and the East Sea/Sea of Japan (Fig. 3h) and then rapidly intensify over the ocean (Figs. 3c, d) presumably due to moisture supply and strong baroclinicity (Hirata et al. 2015).

The individual tracks of Mongolia ETCs are further illustrated in Fig. 4a. Most ETCs are relatively weak over the continent (blue color) but become stronger over the open ocean (red color). They travel not only eastward but also southeastward or northeastward. When traveling southeastward in spring, they can transport Asian dust from Mongolia and North China to the downstream region (e.g., Jung et al. 2019).

The second dominant cyclogenesis is found on the leeward side of the southern Tibetan Plateau (Fig. 3a). The ETCs in this region are referred to as East China ETCs (box “B” in Fig. 3b). As illustrated in Fig. 4b, they travel eastward or northeastward towards the East China Sea and the Kuroshio region then to the Kuroshio-Oyashio extension region. Similar to Mongolia ETCs, East China ETCs grow rapidly over the ocean (Fig. 3d). This result again suggests that the warm ocean plays a crucial role in the development of East Asian ETCs.

Figure 3a further reveals that the Kuroshio region is a central region for coastal cyclogenesis. The ETCs in this region travel along the Kuroshio Current (Fig. 3b) and grow rapidly at the Kuroshio-Oyashio Extension (Figs. 3c, d). These cyclones, hereafter referred to as Kuroshio ETCs, develop by baroclinic instability and diabatic heating (Hirata et al. 2015). As shown in Fig. 4c, Kuroshio ETCs do not always travel eastward along the jet. Many of them also travel northward or northeastward across the jet. These northward-traveling cyclones typically grow more rapidly than those traveling eastward (Hayasaki et al. 2013).

The results shown in Figs. 3 and 4 suggest that East Asian ETCs typically form on the leeward side of the Altai–Sayan Mountains (Mongolia ETCs), the Tibetan Plateau (East China ETCs), and over the Kuroshio region (Kuroshio ETCs), and travel eastward reaching maximum intensity around the Kuroshio–Oyashio Extension. Although ETCs move and grow rather slowly over the continent, they travel faster and become stronger over the ocean. The lifetime of ETCs also becomes longer over the ocean. Most ETCs tend to decay over the Okhotsk Sea (Fig. 3e) where SSTs are low (Fig. 2a).

3.2. Seasonality

Figures 5 and 6 present the seasonal cycle of East Asian ETC properties. The seasonal cycles of ETC frequency and intensity, as examples, are more clearly presented in Fig. 7 and Table 2 for Mongolia, East China, and Kuroshio ETCs.

The left column of Fig. 5 shows that cyclogenesis in East Asia occurs at the geographical fixed locations throughout all seasons. The three major regions of cyclogenesis (i.e., the downstream region of the Altai-Sayan Mountains, the eastern Tibetan Plateau, and over the

Kuroshio region) are robustly found regardless of seasons. Only the number of generated ETCs changes with seasons in each region.

Cyclogenesis is typically maximum in winter (or extended winter) but minimum in summer. Such seasonality is evident over the Kuroshio region. However, continental ETCs exhibit subtle differences between northern and eastern China. The ETC genesis downstream of the Altai-Sayan Mountains is more frequent in fall (SON) than in summer (JJA). However, that of the eastern Tibetan Plateau shows an opposite seasonality with a slightly more frequent cyclogenesis in summer than in fall (compare Figs. 5g, j). This result suggests that the continental ETCs in northern and southern China may have different development processes. Cho et al. (2018) indicated that East China ETCs typically develop with intense diabatic heating. It implies that the seasonality of East China ETC genesis may be related to the strengthening of the diabatic heating by increased moisture supplies in summer.

The middle column of Fig. 5 displays the frequency of ETCs in each season. Although the exact locations of Mongolia, East China, and Kuroshio ETCs are slightly different across the seasons, their existence is prominent. The frequency peaks move slightly equatorward from summer to winter along with an equatorward shift of the westerly jet. Its seasonality, however, is not monotonic in seasons.

Mongolia ETCs are most frequent in spring (Fig. 5e) and fall (Fig. 5k). Their frequencies are even higher than the winter ETC frequency (Fig. 5b). This bimodal seasonality is concisely summarized in Fig. 7a and Table 2. The springtime ETC frequency is approximately 1.1 cyclones per month higher than the wintertime ETC frequency. This difference is approximately 20% of the total wintertime ETC frequency over Mongolia (Table 2). Although less pronounced, ETC frequency over East China is also maximum in spring (Fig. 5b). Quantitatively, East China ETCs are observed approximately 4.8 times per month in the spring but only approximately 4.0 times per month in the winter (Fig. 7b and Table 2). They are not frequent in fall. Figure 5k shows that East China ETCs are not well defined in fall (i.e., no local maxima around box B). This result again suggests that two continental ETCs (i.e., Mongolia and East China ETCs) are not likely organized by the same physical processes.

Kuroshio ETCs are most pronounced in both winter and spring (about to eight ETCs per month) but least in summer (about to five ETCs per month). This seasonality, as summarized in Fig. 7c, is largely explained by the seasonal march of local baroclinicity in the region. Here it is important to note that local cyclogenesis is much smaller than total ETC frequency. The Kuroshio ETCs are locally generated approximately two cyclones per month in winter (Fig. 5a), and one cyclone per month in summer (Fig. 5g). These numbers imply that only 21–30% of ETCs in this region is locally generated, and the majority of ETCs in this region are simply the ones traveling from the continent.

The rightmost column of Fig. 5 shows the seasonal distribution of ETC intensity. As shown in the annual climatology, the maximum intensity appears over the Kuroshio–Oyashio Extension in all seasons. While its seasonality is somewhat similar to that of ETC frequency (compare the middle and right columns in Fig. 5), there is an important difference. Unlike the ETC frequency, ETC intensity is the strongest in spring for all regions (Fig. 5f) and it is different from the seasonality of ETC frequency, which depends on the region. The maximum intensity for East China and Mongolia ETCs is approximately 3.0–3.3 CVU in spring, and this is approximately 0.4–0.7 CVU (about 15–27% of the wintertime cyclone intensity) stronger than that of wintertime ETCs (Figs. 6a, b). Even in the Kuroshio region, spring ETCs are slightly stronger than winter ETCs (Figs. 5c, f).

It is unclear why East Asian ETC activities are strongest in spring than in winter. However, this seasonality is consistent with the midwinter suppression of the Pacific storm track (Nakamura 1992). A series of studied have shown that Pacific storm track activities in midwinter, when local baroclinicity is maximum, are weaker than those in spring (Nakamura 1992; Chang et al. 2002; Penny et al. 2010). It is likely associated with jet intensity, shape, and/or diabatic heating. But its mechanism(s) remains to be determined.

Figure 6 further illustrates ETC growth rate (left), decay rate (middle), and cyclolysis (right) in each season. Similar to climatology (Fig. 3d), growth rate is high over Mongolia, Yangtze River, and the Kuroshio-Oyashio extension (Figs. 6a, d, g, and j). East Asian ETCs grow fastest over the Kuroshio-Oyashio extension, slightly upstream of maximum ETC intensity (Figs. 5c, f, and i). Their growth rate is maximum in winter (greater than 3.1 CVU per day) when SST is relatively warm, and its meridional gradient is sharp, but minimum in summer (about 1.3 CVU per day). Around Mongolia, ETCs grow faster in spring (higher than 1.6 CVU per day) than in summer (about 1.3 CVU per day). Although growth rate is also high in fall and winter, the region of high growth rate is narrow. The East China ETCs typically strengthen around Yangtze River with a maximum growth rate in spring but a minimum rate in fall as in cyclogenesis (Figs. 5a, d, g, and j).

The decay rate is further illustrated in Figs. 6b, e, h, and k. Overall decay rate is high in the Okhotsk Sea, downstream of the rapid ETC growth region (compare the left and middle columns in Fig. 6). This indicates that rapidly developing ETCs over the Kuroshio–Oyashio Extension tend to decay over the cold ocean as they travel northeastward. However, only few ETCs dissipate in this region. As shown in the rightmost column of Fig. 6, cyclolysis mainly occurs along the coastline of the continent rather than over the cold ocean. The decaying ETCs in this region, maximum of 1.5 cyclones per month, are typically those traveling in the continent or those landing from the ocean. Note that this does not necessarily represent the cyclolysis of East Asian ETCs but any ETCs traveling across the analysis domain. The cyclolysis of many East Asian ETCs occurs in the Gulf of Alaska (Sinclair 1997; Hoskins and Hodges 2002).

The seasonal evolutions of ETC lifetime, traveling speed and distance are also examined (Fig. S1). It is found that winter ETCs have a relatively short lifetime, moving fast over the ocean. The summer ETCs, although weak and less frequent, are maintained one or two days longer than the winter ETCs in most regions. Moreover, they travel slowly (about 30 km per hour) because of weak background flow. Most ETCs travel more than 4,000 km in the analysis domain.

3.3. Long-term variability

The above result reveals that East Asian ETCs have different climatic features depending on the season and region. Although not examined in detail, they also exhibit considerable temporal variability. Table 2 concisely summarizes the interannual variability of ETC frequency. The number of East Asian ETCs varies about 10–20% from one year to another. Mongolia ETCs (approximately 8–13% variability with respect to the mean frequency) have relatively small interannual variation compared with East China ETCs (11–19%) and Kuroshio ETCs (9–20%). The largest variability, which is observed in Kuroshio ETCs in fall, is about one cyclone per month, although its reason is unclear.

Figure 8 presents the long-term trends of ETC frequency (see also the parenthesized number in Table 2). East Asian ETC frequency shows a slightly negative trend in most seasons and most regions (not shown). However, overall trends are largely statistically insignificant. Two exceptions are springtime East China ETCs (blue shading in Fig. 8b) and summertime Mongolia ETCs (Fig. 8c). Their trends are -0.16 and -0.27 cyclones per decade respectively, corresponding to about 3.3% and 5.2% reduction of ETC frequency per decade in each region. Such changes, which are marginally significant at the 95% confidence level, are mainly due to reduced cyclogenesis (not shown). Although not shown, the overall intensities of these ETCs do not change much.

Figure 9 shows the time evolution of the summertime Mongolia ETC frequency and the springtime East China ETC frequency. The top-50% ETCs in intensity are also separately shown. It turns out that only relatively weak ETCs have decreased over Mongolia (Fig. 9a). The top-50% ETCs show essentially no trends, indicating that large-scale circulation changes may have different impacts on weak and strong ETCs. Unlike Mongolia ETCs, East China ETCs have systematically decreased over the analysis period (Fig. 9b).

What causes declining trends in ETC frequency? Cho et al. (2018) argued that the reduction in East China ETC frequency is partly caused by weakened moisture flux convergence in response to enhanced warm-pool convection over the Maritime Continent and the Philippines Sea during the last four decades. Note that the Gill-type response (Gill 1980) to the enhanced tropical convection results in a strengthened moisture flux convergence over southeast China and the East China Sea, but a weakened moisture flux convergence over southwest China where East China ETCs develop. Unlike East China ETCs, the long-term trends of summertime Mongolia ETCs are not well addressed in the literature. It is particularly true for observations. Although Loptien et al. (2008) showed that summertime ETC frequency over Mongolia would decrease under future climate scenarios by performing coupled model experiments, the driving mechanism(s) has not been identified.

It is anticipated that ETC-frequency trends, shown in Fig. 8, are at least partly caused by the long-term changes in atmospheric circulation. To better understand a declining ETC frequency in East Asia, the long-term trends of westerly jet (zonal wind at 300 hPa) and static stability, which are the two key factors for baroclinic instability, are examined in Fig. 10. The springtime jet stream does not show any significant trend (Fig. 10a). Although a weak negative trend is observed in summer, the trend in the downstream region of the Tibetan Plateau is confined to the narrow region (Fig. 10b). This result suggests that ETC-frequency change is not likely caused by vertical wind shear change.

Figures 10c and d show the bulk static stability change in the two seasons. The bulk static stability is computed by potential temperature difference between 300- and 700-hPa pressure levels. In spring, the stability has significantly increased in the subtropics from northern India to southern Japan (Fig. 10c). The stability has also increased in summer but mostly in northern China (Fig. 10d). These regions of enhanced stability, presumably due to global warming, coincide with those of reduced ETC frequency, indicating that ETC activity change in East Asia is likely associated with background static stability change. To better understand the physical mechanism(s), further investigations, especially using numerical model, would be needed.

4. Summary and Discussion

This study documents the climatological properties of East Asian ETCs that are detected and tracked with an automated tracking algorithm applied to an 850-hPa relative vorticity field. East Asian ETCs exhibit three regions of maximum cyclogenesis (i.e., Mongolia, East China, and the Kuroshio Current region). Developing cyclones typically form in the downstream region of mountains (e.g., Mongolia and East China ETCs) and over the Kuroshio region (Kuroshio ETCs). While the former ETCs are generated by lee cyclogenesis, the latter ETCs are organized by baroclinic instability and diabatic processes. The results are consistent with the previous studies (Adachi and Kimura 2007; Zhang et al. 2012; Chen et al. 2014).

The East Asian ETCs commonly strengthen with time but have somewhat different seasonality. Both Mongolia and East China ETCs show a maximum frequency and intensity in spring rather than in winter. The highest frequency and intensity in spring are one of the prominent features of East Asian ETCs, compared to North America where ETC frequency and intensity are maximum in winter (e.g., Zishka and Smith 1980). While Mongolia ETCs are also frequent in fall, East China ETCs are not well defined in fall. This implies that development mechanisms of these two ETCs may differ with seasons. The Kuroshio ETCs also exhibit a maximum intensity in spring, but their frequency is maximum in winter. It is unclear why East Asian ETC activities are prominent in spring. But this result is consistent with the midwinter suppression of the Pacific storm track (Nakamura 1992), implying that a relatively weaker Pacific storm track in winter than in spring is partly caused by East Asian ETC activities on its upstream region.

Most East Asian ETCs rapidly grow over the Kuroshio–Oyashio extension as they travel eastward or northeastward, then decay over the Okhotsk Sea. A maximum growth over the Kuroshio-Oyashio extension is observed in winter, whereas a maximum decay over the Okhotsk Sea is found in spring. This seasonality is slightly different from the ETCs over the North Pacific which grow and decay strongly in cold season (Martin et al. 2001). In winter, East Asian ETCs have a relatively short lifetime and move fast over a long distance. Compared with them, summer ETCs are maintained longer and move slower because of weak background flow.

The interannual variabilities of East Asian ETCs are about 10–20% of mean frequencies, depending on seasons and their origins. A part of this interannual variability is likely associated with ENSO. Although not shown, a preliminary analysis of the year-to-year variability of wintertime ETCs shows that East Asian ETCs are more active during El Niño winters than during La Niña winters. This is particularly true for East China ETC frequency. The El Niño-related ETC activities are also pronounced in the south of Japan. As discussed in Ueda et al. (2017), ETC frequency in this region significantly increases during El Niño winters because of a weakened subtropical jet. Note that a strong subtropical jet tends to suppress cyclogenesis in this region (Nakamura and Sampe 2002).

In term of the long-term trend, East Asian ETCs show a hint of the decreasing trend in their frequency. Only continental ETCs exhibit marginally significant trends in the two seasons. In particular, the numbers of Mongolia and East China ETCs have decreased in summer and in spring, respectively. Although the detailed dynamic mechanism(s) remains to be determined, this trend is at least consistent with an enhanced static stability in the region which is caused by global warming.

To better understand East Asian ETC properties, an extended study is needed. Among others, intraseasonal to interannual variabilities need to be addressed as in Grise et al. (2013). For instance, ETC modulations by Asian summer and winter monsoons, Pacific-North American teleconnection, Madden-Julian Oscillation, and circumglobal teleconnection deserve further analyses. The detailed development and decaying mechanisms of Mongolia, East China and Kuroshio ETCs, as well as their long-term trends, also need further investigations. These issues will be addressed in future studies.

This is a post-peer-review, pre-copyedit version of an article published in Climate Dynamics. The final authenticated version is available online at: https://doi.org/10.1007/s00382-019-05048-w

Acknowledgements

We thank Jung Choi, Joon-Woo Roh, Joonsuk M. Kang, and Enoch Jo for their helpful comments. This study was funded by the National Research Foundatioin of Korea (NRF) grant funded by the Korean government (MSIT) (NRF-2018R1A5A1024958), Swedish Research Council VR (2014-1864), and the Numerical Modeling Center from the Korea Meteorological Administration Research and Development Program for the Next Generation Model Development Project through grant 1365003079.

References

Adachi S, Kimura F (2007) A 36-year climatology of surface cyclogenesis in East Asia using high-resolution reanalysis data. SOLA 3:113-116, doi: 10.2151/sola.2007-029

Bengtsson L, Hodges KI, Roeckner E (2006) Storm tracks and climate change. J Clim 19:3518-3543. doi:10.1175/JCLI3815.1

Côté H, Grise KM, Son S-W, de Elía R, Frigon A (2015) Challenges of tracking extratropical cyclones in regional climate models. Clim Dyn 44:3101-3109. doi:10.1007/s00382-014-2327-x

Chang EK, Lee S, Swanson KL (2002) Storm track dynamics. J Clim 15:2163-2183. doi: 10.1175/1520-0442(2002)015<02163:STD>2.0.CO;2

Chen L, Tan B, Kvamstø NG, Johannessen OM (2014) Wintertime cyclone/anticyclone activity over China and its relation to upper tropospheric jets. Tellus 66A:21889. doi:10.3402/tellusa.v66.21889

Chen S-J, Lazić L (1990) Numerical case study of the Altai-Sayan lee cyclogenesis over east Asia. Meteorol Atmos Phys 42:221-229. doi:10.1007/BF01314826

This is a post-peer-review, pre-copyedit version of an article published in Climate Dynamics. The final authenticated version is available online at: https://doi.org/10.1007/s00382-019-05048-w

Chen S-J, Kuo Y-H, Zhang P-Z, Bai Q-F (1991) Synoptic climatology of cyclogenesis over East Asia, 1958-1987. Mon Weather Rev 119:1407-1418. doi:10.1175/15200493(1991)119<1407:SCOCOE>2.0.CO;2

Chen S-J, Kuo Y-H, Zhang P-Z, Bai Q-F (1992) Climatology of explosive cyclones off the East Asian coast. Mon Weather Rev 120:3029-3035. doi:10.1175/1520-0493(1992)120<3029:COECOT>2. 0.CO;2

Cho H-O, Son S-W, Park D-SR (2018) Springtime extratropical cyclones in Northeast Asia and their impacts on long-term precipitation trends. Int J Climatol 38(10):4043-4050. doi: 10.1002/joc.5543

Chung Y-S, Hage KD, Reinelt ER (1976) On lee cyclogenesis and airflow in the Canadian Rocky Mountains and the East Asian Mountains. Mon Weather Rev 104:879-891. doi:10.1175/1520-0493(1976)104<0879:OLCAAI>2.0.CO;2

Dee DP et al (2011) The ERA-Interim reanalysis: configuration and performance of the data assimilation system. Q J R Meteorol Soc **137**:553–597. doi:10.1002/qj.828

Dong B, Sutton RT, Woollings T, Hodges K (2013) Variability of the North Atlantic summer storm track: meachanisms and impacts on the European climate. Environ Res Lett 8(034):037. doi: 10.1088/1748-9326/8/3/034037

Gagen MH, Zorita E, McCarroll D, Zahn M, Young GH, Robertson I (2016) North Atlantic summer storm tracks over Europe dominated by internal variability over the past millennium. Nat Geosci 9(8):630.

Gill AE (1980) Some simple solutions for heat-induced tropical circulation. Q J R Meteorol Soc 106(449):447-462

Grise KM, Son S-W, Gyakum JR (2013) Intraseasonal and interannual variability in North American storm tracks and its relationship to equatorial Pacific variability. Mon Weather Rev 141:3610-3625. doi:10.1175/MWR-D-12-00322.1

Hayasaki M, Kawamura R, Mori M, Watanabe M (2013) Response of extratropical cyclone activity to the Kuroshio large meander in northern winter. Geophys Res Lett 40:2851-2855. doi: 10.1002/grl.50546

Hirata H, Kawamura R, Kato M, Shinoda T (2015) Influential Role of Moisture Supply from the Kuroshio/Kuroshio Extension in the Rapid Development of an Extratropical Cyclone. Mon Weather Rev 143:4126-4144. doi:10.1175/MWR-D-15-0016.1

Hodges KI (1994) A general-method for tracking analysis and its application to meteorological data. Mon Weather Rev 122:2573-2586. doi:10.1175/1520-0493(1994)122<2573:AGMFTA> 2.0.CO;2

Hodges KI (1995) Feature tracking on the unit sphere. Mon Weather Rev 123:3458-3465. doi:10.1175 /1520-0493(1995)123<3458:FTOTUS>2.0.CO;2

Hodges KI (1999) Adaptive constraints for feature tracking. Mon Weather Rev 127:1362-1373. doi:10. 1175/1520-0493(1999)127<1362:ACFFT>2.0.CO;2

Hoskins BJ, Hodges KI (2002) New perspectives on the Northern Hemisphere winter storm tracks. J Atmos Sci 59:1041-1061, doi:10.1175/1520-0469(2002)059<1041:NPOTNH>2.0.C O;2

Hoskins BJ, Valdes P (1990) On the existence of storm-tracks. J Atmos Sci 47:1854–64.

Huang B et al (2015) Extended reconstructed sea surface temperature version 4 (ERSST. v4). Part I: upgrades and intercomparisons. J Clim 28:931–951. doi:10.1175/JCLI-D-14-00006.1

This is a post-peer-review, pre-copyedit version of an article published in Climate Dynamics. The final authenticated version is available online at: https://doi.org/10.1007/s00382-019-05048-w

Inatsu M (2009) The neighbor enclosed area tracking algorithm for extratropical wintertime cyclones. Atmos Sci Lett 10:267-272. doi:10.1002/asl.238

Iwao K, Inatsu M, Kimoto M (2012) Recent changes in explosively developing extratropical cyclones over the winter Northwestern Pacific. J Clim 25:7282-7296. doi:10.1175/JCLI-D-11-00373.1

Jung M-I, Son S-W, Kim HC, Kim S-W, Park RJ, Chen D (2019) Comparison of synoptic weather patterns between non-dust high particulate matter and Asian dust events observed in Seoul, South Korea. Submitted.

Lindzen R, Farrell B (1980) A simple approximate result for the maximum growth rate of baroclinic instabilities. J Atmos Sci 37:1648–54.

Loptien U, Zolina O, Gulev S, Latif M, Soloviov V (2008) Cyclone life cycle characteristics over the Northern Hemisphere in coupled GCMs. Clim Dyn 31:507-532. doi:10.1007/s00382-007-0355-5

Nakamura H (1992) Midwinter suppression of baroclinic wave activity in the Pacific. J Atmos Sci 49:1629-1642. doi:10.1175/1520-0469(1992)049<1629:MSOBWA>2.0.CO;2

Nakamura H, Sampe T (2002) Trapping of synoptic-scale disturbances into the North-Pacific subtropical jet core in midwinter. Geophys Res Lett 29(16):8-1. doi:10.1029/2002GL015535

Neu U et al (2013) IMILAST: a community effort to intercompare extratropical cyclone detection and tracking algorithms. Bull Am Meteorol Soc 94:529–547. doi:10.1175/BAMS-D-11-00154.1

Martin JE, Grauman RD, Marsili N (2001) Surface cyclolysis in the North Pacific Ocean. Part I: A synoptic climatology. Mon Weather Rev 129(4):748-765.

Mesquita, MDS, Atkinson DE, Hodges KI (2010) Characteristics and variability of storm tracks in the North Pacific, Bering Sea, and Alaska. J Clim 23(2):294-311.

Mesquita MDS, Kvamstø NG,Sorteberg A, Atkinson DE (2008) Climatological properties of summertime extra-tropical storm tracks in the Northern Hemisphere. Tellus 60A:557–569.

Penny S, Roe GH, Battisti DS (2010) The source of the midwinter suppression in storminess over the North Pacific. J Clim 23(3):634-648. doi: 10.1175/2009JCLI2904.1

Plante M, Son S-W, Atallah E, Gyakum JR, Grise KM (2014) Extratropical cyclone climatology across eastern Canada. Int J Climatol 35:2759-2776. doi:10.1002/joc.4170

Rosenfeld A, AC Kak (1976) *Digital Picture Processing*. Academic Press.

Sanders F, Gyakum JR (1980) Synoptic-dynamic climatology of the “bomb”. Mon Weather Rev 108:1589-1606. doi:10.1175/1520-0493(1980)108<1589:SDCOT>2.0.CO;2

Sinclair MR (1997) Objective identification of cyclones and their circulation intensity and climatology. Wea Forecasting 12:595–612.

Uccellini LW, Kocin PJ (1987) The interaction of jet streak circulations during heavy snow events along the east coast of the United States. Wea Forecasting 2:289-308. doi:10.1175/1520-0434(1987)002<0289:TIOJSC>2.0.CO;2

Ueda H, Amagai Y, Hayasaki M (2017) South-coast cyclone in Japan during El Niño-caused warm winters. Asia-Pac J Atmospheric Sci 53(2):287-293. doi:10.1007/s13143-017-0025-4

Wang X, Zhai P, Wang C (2009) Variations in extratropical cyclone activity in northern East Asia. Adv Atmos Sci 26:471-479. doi:10.1007/s00376-009-0471-8

Whittaker LM, Horn LH (1984) Northern Hemisphere extratropical cyclone activity for four mid-season months. Int J Climatol 4:297-310. doi: 10.1002/joc.3370040307

This is a post-peer-review, pre-copyedit version of an article published in Climate Dynamics. The final authenticated version is available online at: https://doi.org/10.1007/s00382-019-05048-w

Yoshida A, Asuma Y (2004) Structures and environment of explosively developing extratropical cyclones in the northwestern Pacific region. Mon Weather Rev 132:1121-1142. doi: 10.1175/1520-0493(2004)132<1121:SAEOED>2.0.CO;2

Zappa G, Shaffrey LC, Hodges KI (2013a) The ability of CMIP5 models to simulate North Atlantic extratropical cyclones. J Clim 26:5379-5396. doi:10.1175/JCLI-D-12-00501.1

Zappa G, Shaffrey LC, Hodges KI, Sansom PG, Stephenson DB (2013b) A multimodel assessment of future projections of North Atlantic and European extratropical cyclones in the CMIP5 climate models. J Clim 26:5846-5862. doi:10.1175/JCLI-D-12-00573.1

Zhang Y, Ding Y, Li Q (2012) A climatology of extratropical cyclones over East Asia during 1958–2001. Acta Meteor Sin 26:261-277. doi:10.1007/s13351-012-0301-2

Zishka KM., Smith PJ (1980) The climatology of cyclones and anticyclones over North America and surrounding ocean environs for January and July, 1950–77. Mon Wea Rev 108(4):387-401.

Table caption list

Table 1. Definition of ETC properties.

Table 2. The long-term mean and interannual variability (one standard deviation) of ETC frequency over Mongolia, East China, and the Kuroshio Current region. Long-term trend is indicated in parenthesis. The trend that is statistically significant at the 95% confidence level is denoted with an asterisk.

Figure caption list

Fig. 1. The analysis domain. The light grey lines over the continent indicates 1.5-km high elevation.

Fig. 2. (a) Sea surface temperature distribution (shaded; in °C), (b) climatological zonal wind at 300-hPa pressure level (in m s^{-1}), and (c) Eady growth rate (in day^{-1}). The light grey shading over the continent indicates 1.5-km high elevation.

Fig. 3. Climatology of East Asian ETCs: (a) cyclogenesis (in # $month^{-1}$), (b) frequency (in # $month^{-1}$), (c) intensity (in CVU), (d) growth rate (in CVU day^{-1}), (e) decay rate (in CVU day^{-1}), (f) cyclolysis (in # $month^{-1}$), (g) lifetime (in day), (h) speed (in km h^{-1}), and (i) traveling distance (in 10^3 km). See Table 1 for the definition and unit of each property. All ETC properties are only

considered for the grid points where one or more ETCs are present. Three black boxes in (b) represent (box A) Mongolia, (box B) East China, and (box C) Kuroshio Current domain.

Fig. 4. Individual ETC tracks that start from the leeward sides of (a) the Altai–Sayan Mountains and (b) the Tibetan Plateau, and (c) from the Kuroshio Current region. The color represents ETC intensity in CVU. The black box in each plot indicates the domain where the initial ETCs are located.

Fig. 5. Seasonal cycles of (left) cyclogenesis (in # month^{-1}), (middle) frequency (in # month^{-1}), and (right column) intensity (in CVU) of East Asian ETCs in (first) winter, (second) spring, (third) summer, and (fourth row) fall

Fig. 6. Seasonal cycles of (left) growing rate (in CVU day^{-1}), (middle) decaying rate (in CVU day^{-1}), and (right column) cyclolysis (in # month^{-1}) of East Asian ETCs in (first) winter, (second) spring, (third) summer, and (fourth row) fall.

Fig. 7. Long-term mean Seasonal cycle of ETC frequency (blue bars) and intensity (orange bars) in the three cyclogenesis regions shown in Fig. 2a. The error bar indicates the interannual variation at one standard deviation.

Fig. 8. Seasonal-mean ETC frequency (contours; identical to the middle column of Fig. 4) and its long-term trend (shaded; in number of ETCs per decade). Only trends that are statistically significant at the 95% confidence level are shown.

Fig. 9. Time series of ETC frequency and its linear trend for (a) summertime Mongolia ETCs and (b) springtime East China ETCs over the period of 1979–2017. Top 50% ETCs in intensity are separately shown. The solid red lines indicate statistically significant trends at the 95% confidence level.

This is a post-peer-review, pre-copyedit version of an article published in Climate Dynamics. The final authenticated version is available online at: https://doi.org/10.1007/s00382-019-05048-w

Fig. 10. Seasonal-mean (contours) and decadal trends (shaded) of 300-hPa zonal wind (top; in m s^{-1} dec^{-1}) and bulk static stability (bottom; in K dec^{-1}) in spring (left) and summer (right). Bulk static stability is defined by potential temperature difference between at the 300- and 700-hPa pressure levels. The trends that are statistically significant at the 95% confidence level are denoted with dots.

Supplementary figure caption list

Fig. S1. Seasonal cycles of (left) lifetime (in day), (middle) speed (in km h^{-1}), and (right column) travel distance (in 10^3 km) of East Asian ETCs in (first) winter, (second) spring, (third) summer, and (fourth row) fall.

Table 1. Definition of ETC properties.

ETC Property (unit)	Description
Cyclogenesis (# $month^{-1}$)	The initial point of the detected cyclones (or the first location where ETC intensity becomes stronger than 1 CVU) within 555-km radius at each grid point.
Frequency (# $month^{-1}$)	The number of cyclones within 555-km radius at each grid point. For each grid point, same cyclone is counted only once.
Intensity (CVU)	The mean intensity of the detected cyclones within 555-km radius at each grid point. The intensity is defined as the local maximum of 850-hPa relative vorticity.

Growth rate ($CVU\ day^{-1}$)	The positive value of intensity difference between ±6 hours within 555-km radius at each grid point.
Decay rate ($CVU\ day^{-1}$)	The negative value of intensity difference between ±6 hours within 555-km radius at each grid point.
Cyclolysis ($\#\ month^{-1}$)	The last point of the detected cyclones (or the location where ETC intensity becomes weaker than 1 CVU) within 555-km radius at each grid point.
Lifetime (day)	The time span from cyclogenesis to cyclolysis within 555-km radius at each grid point.
Speed ($km\ h^{-1}$)	The distance that each cyclone traveled in each time step within 555-km radius at each grid point divided by 6 hours.
Traveling distance (10^3 km)	The traveling distance of cyclone that maintains a minimum intensity of 1 CVU within 555-km radius at each grid point.

Table 2. The long-term mean and interannual variability (one standard deviation) of ETC frequency over Mongolia, East China, and the Kuroshio Current region. Long-term trend is indicated in parenthesis. The trend that is statistically significant at the 95% confidence level is denoted with an asterisk.

	Mongolia ETCs	**East China ETCs**	**Kuroshio ETCs**
DJF	5.37±0.62 ($0.01\ dec^{-1}$)	3.97±0.67 ($-0.14\ dec^{-1}$)	7.31±0.78 ($-0.13\ dec^{-1}$)

MAM	6.46±0.53 (-0.01 dec^{-1})	4.81±0.52 (-0.16* dec^{-1})	7.06±0.66 (-0.03 dec^{-1})
JJA	5.20±0.69 (-0.27* dec^{-1})	3.23±0.66 (0.00 dec^{-1})	5.03±0.88 (-0.06 dec^{-1})
SON	6.00±0.57 (-0.11 dec^{-1})	2.89±0.48 (-0.06 dec^{-1})	5.40±1.01 (0.01 dec^{-1})

This is a post-peer-review, pre-copyedit version of an article published in Climate Dynamics. The final authenticated version is available online at: https://doi.org/10.1007/s00382-019-05048-w

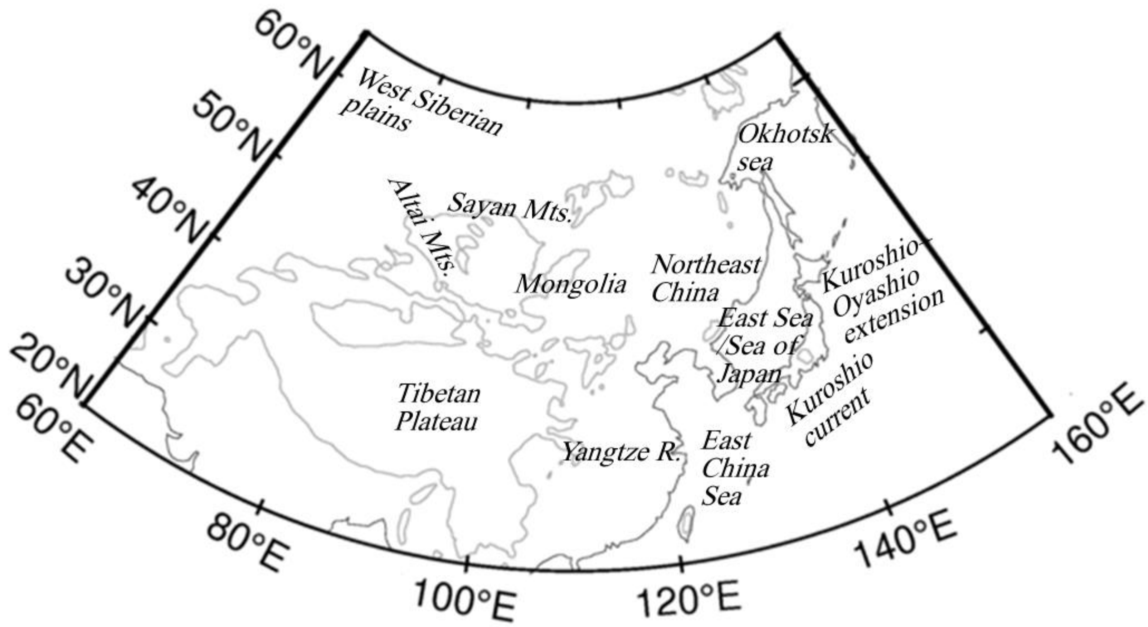

641 Fig. 1. The analysis domain. The light grey lines over the continent indicates 1.5-km high
642 elevation.

This is a post-peer-review, pre-copyedit version of an article published in Climate Dynamics. The final authenticated version is available online at: https://doi.org/10.1007/s00382-019-05048-w

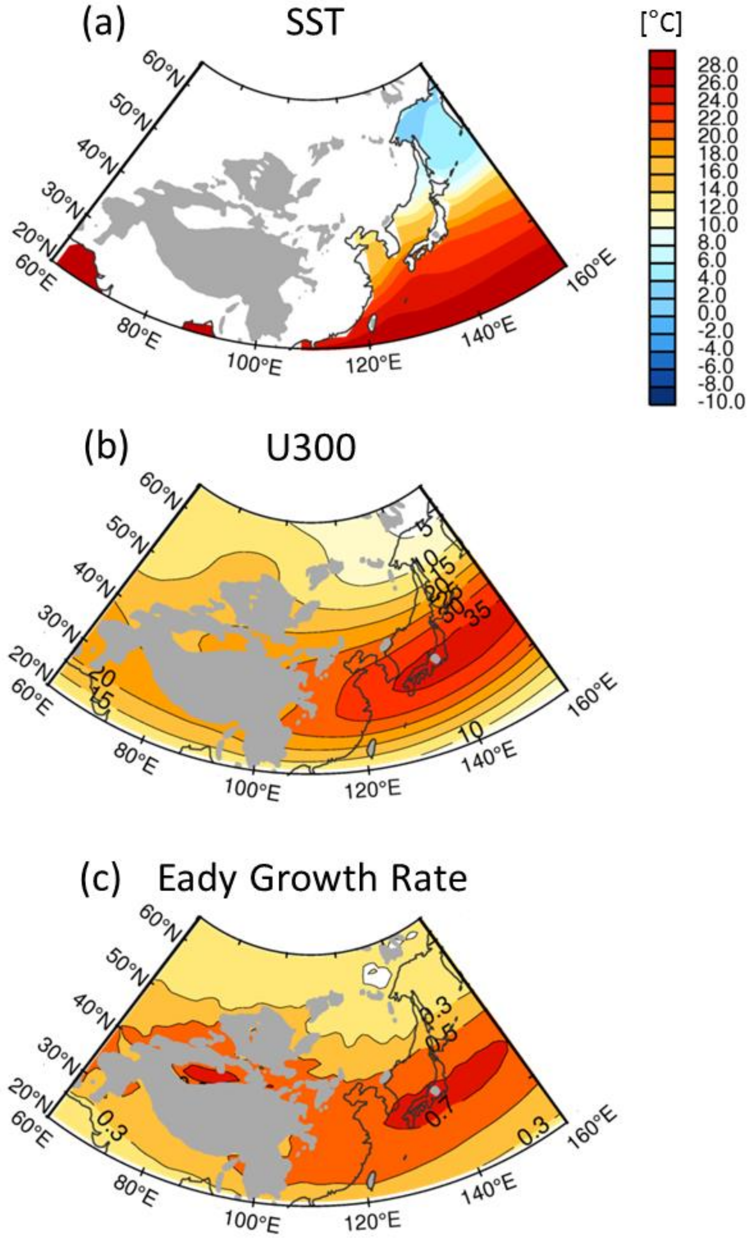

Fig. 2. (a) Sea surface temperature distribution (shaded; in °C), (b) climatological zonal wind at 300-hPa pressure level (in m s^{-1}), and (c) Eady growth rate (in day^{-1}). The light grey shading over the continent indicates 1.5-km high elevation.

This is a post-peer-review, pre-copyedit version of an article published in Climate Dynamics. The final authenticated version is available online at: https://doi.org/10.1007/s00382-019-05048-w

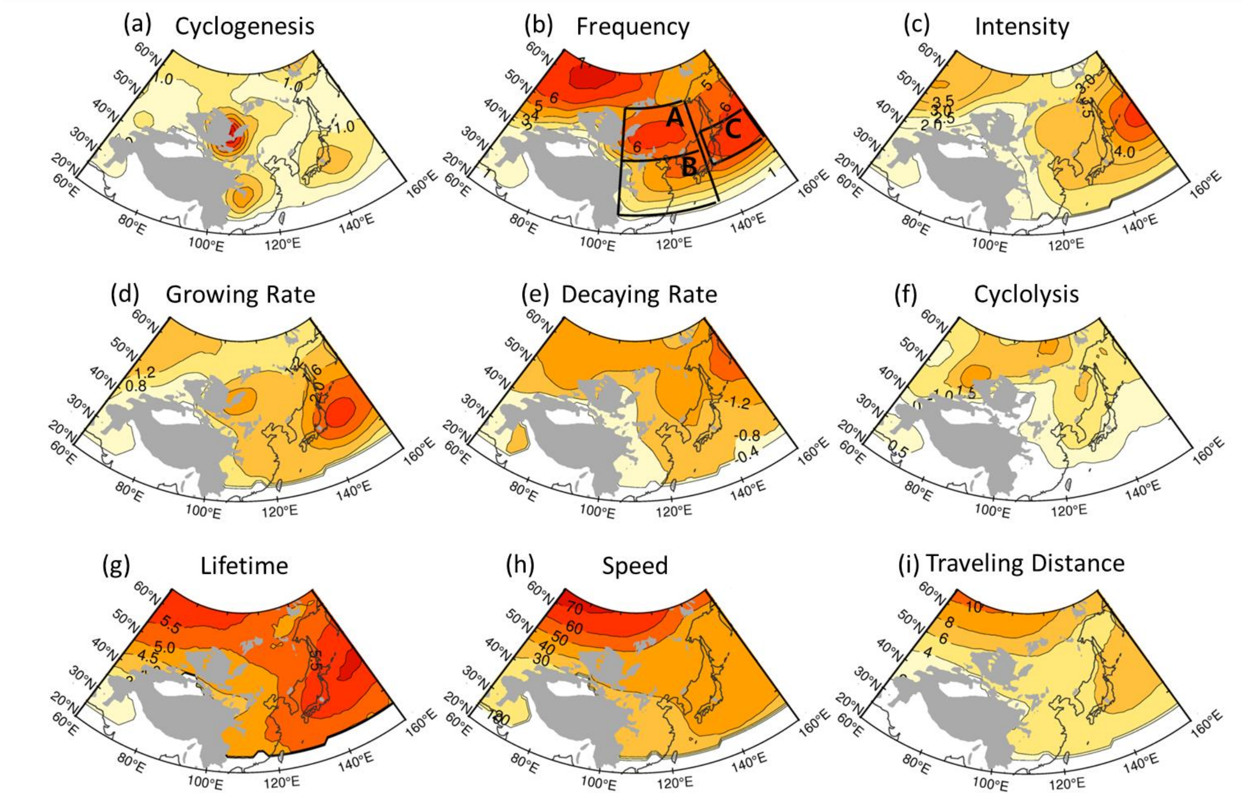

Fig. 3. Climatology of East Asian ETCs: (a) cyclogenesis (in # month^{-1}), (b) frequency (in # month^{-1}), (c) intensity (in CVU), (d) growth rate (in CVU day^{-1}), (e) decay rate (in CVU day^{-1}), (f) cyclolysis (in # month^{-1}), (g) lifetime (in day), (h) speed (in km h^{-1}), and (i) traveling distance (in 10^3 km) from 1979 to 2017. See Table 1 for the definition and unit of each property. All ETC properties are only considered for the grid points where one or more ETCs are present. Three black boxes in (b) represent (box A) Mongolia, (box B) East China, and (box C) Kuroshio Current domain.

This is a post-peer-review, pre-copyedit version of an article published in Climate Dynamics. The final authenticated version is available online at: https://doi.org/10.1007/s00382-019-05048-w

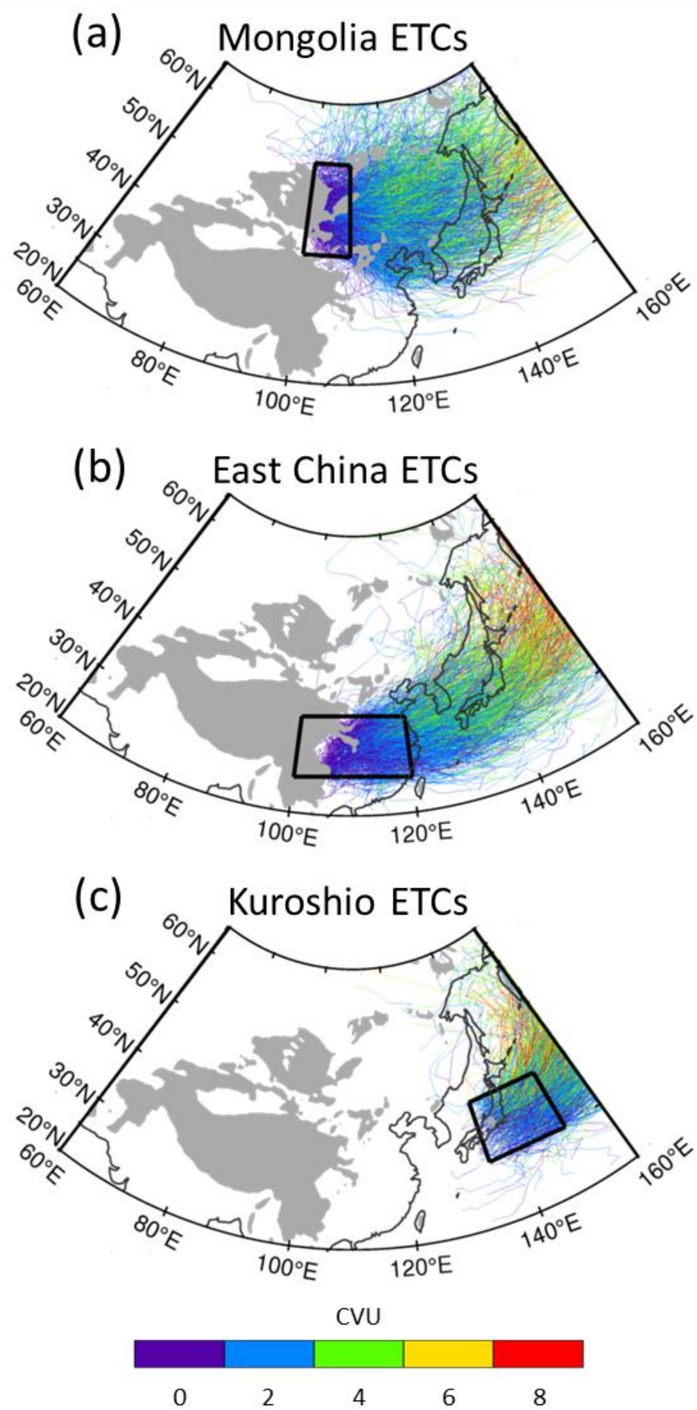

Fig. 4. Individual ETC tracks that start from the leeward sides of (a) the Altai–Sayan Mountains and (b) the Tibetan Plateau, and (c) from the Kuroshio Current region. The color represents ETC

intensity in CVU. The black box in each plot indicates the domain where the initial ETCs are located.

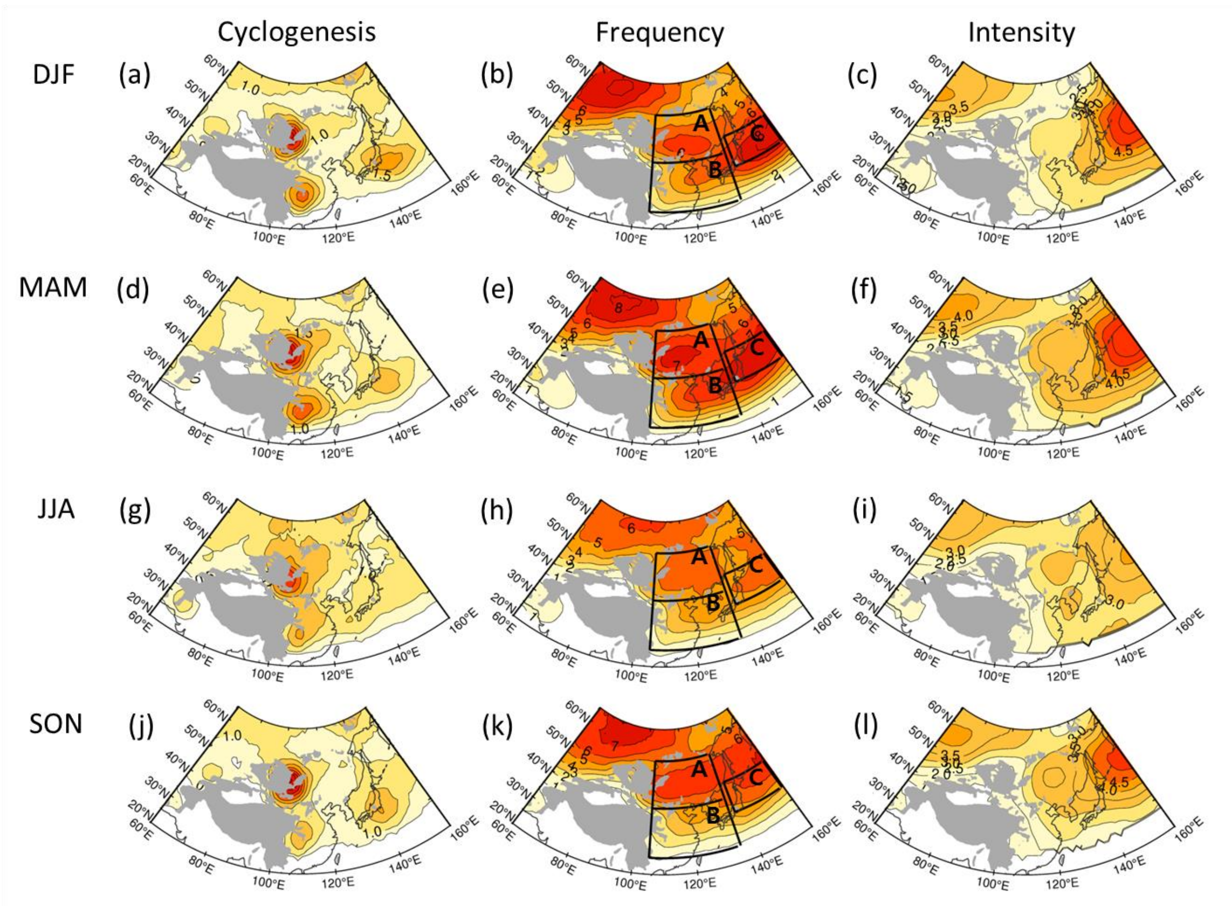

Fig. 5. Seasonal cycles of (left) cyclogenesis (in # month^{-1}), (middle) frequency (in # month^{-1}), and (right column) intensity (in CVU) of East Asian ETCs in (first) winter, (second) spring, (third) summer, and (fourth row) fall.

This is a post-peer-review, pre-copyedit version of an article published in Climate Dynamics. The final authenticated version is available online at: https://doi.org/10.1007/s00382-019-05048-w

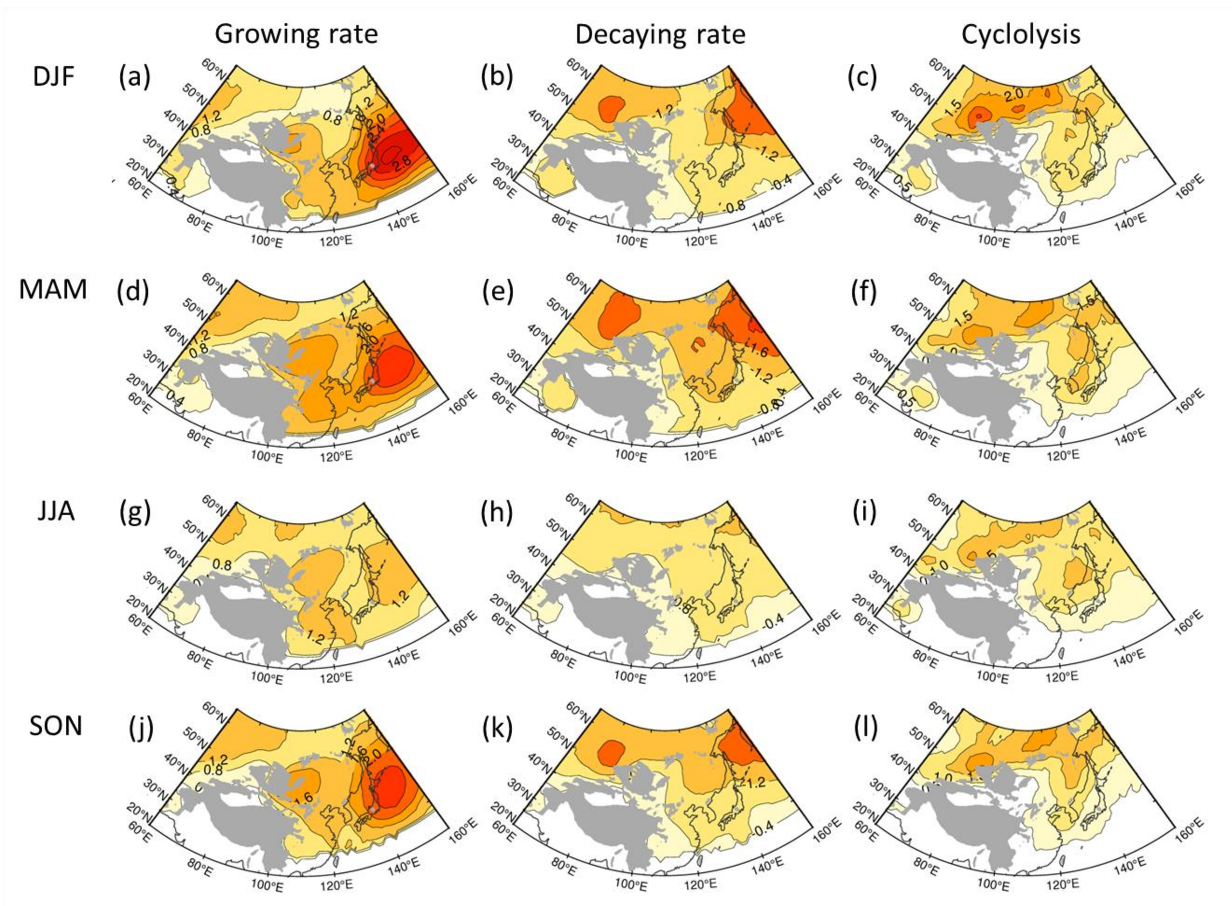

Fig. 6. Seasonal cycles of (left) growing rate (in CVU day^{-1}), (middle) decaying rate (in CVU day^{-1}), and (right column) cyclolysis (in # month^{-1}) of East Asian ETCs in (first) winter, (second) spring, (third) summer, and (fourth row) fall.

This is a post-peer-review, pre-copyedit version of an article published in Climate Dynamics. The final authenticated version is available online at: https://doi.org/10.1007/s00382-019-05048-w

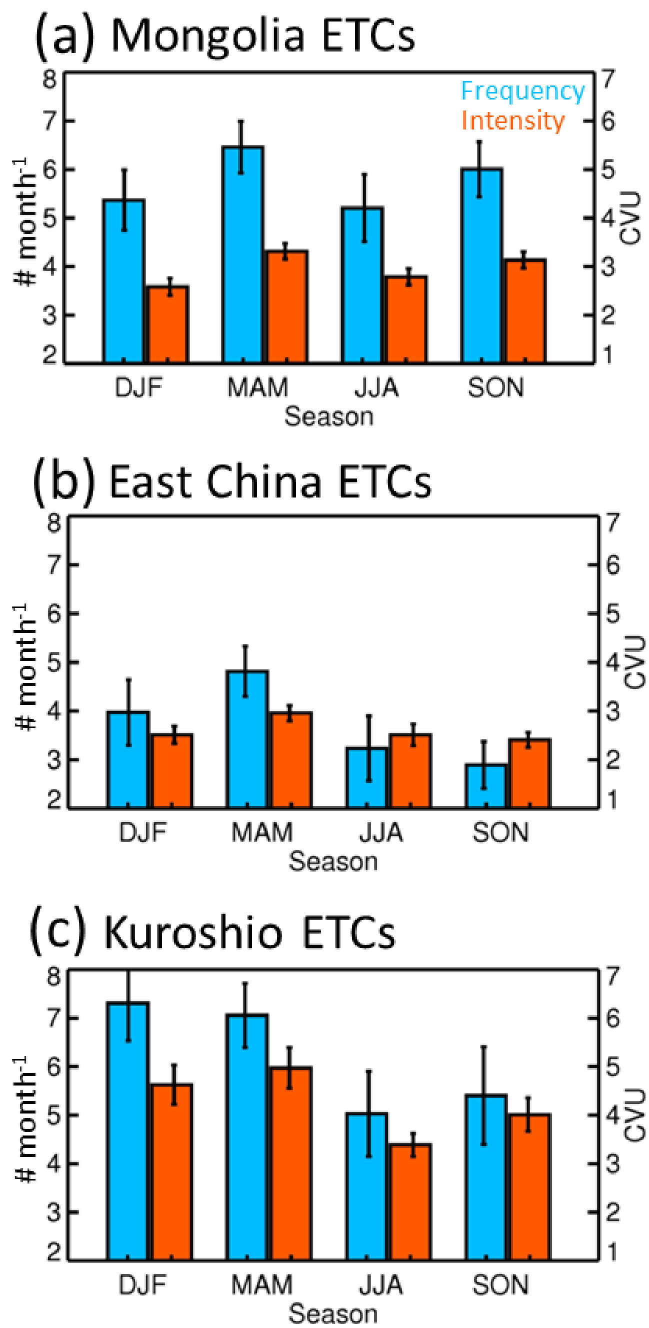

Fig. 7. Long-term mean Seasonal cycle of ETC frequency (blue bars) and intensity (orange bars) in the three cyclogenesis regions shown in Fig. 2a. The error bar indicates the interannual variation at one standard deviation.

This is a post-peer-review, pre-copyedit version of an article published in Climate Dynamics. The final authenticated version is available online at: https://doi.org/10.1007/s00382-019-05048-w

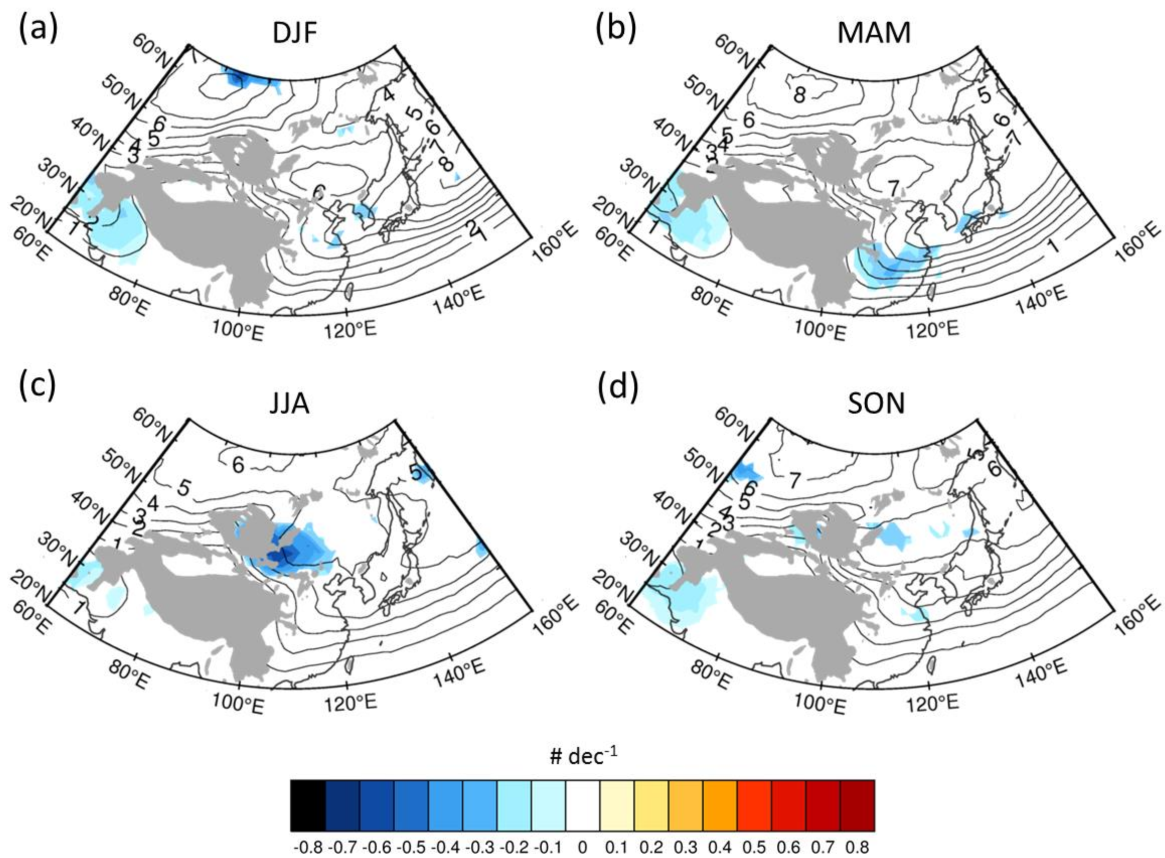

Fig. 8. Seasonal-mean ETC frequency (contours; identical to the middle column of Fig. 4) and its long-term trend (shaded; in number of ETCs per decade). Only trends that are statistically significant at the 95% confidence level are shown.

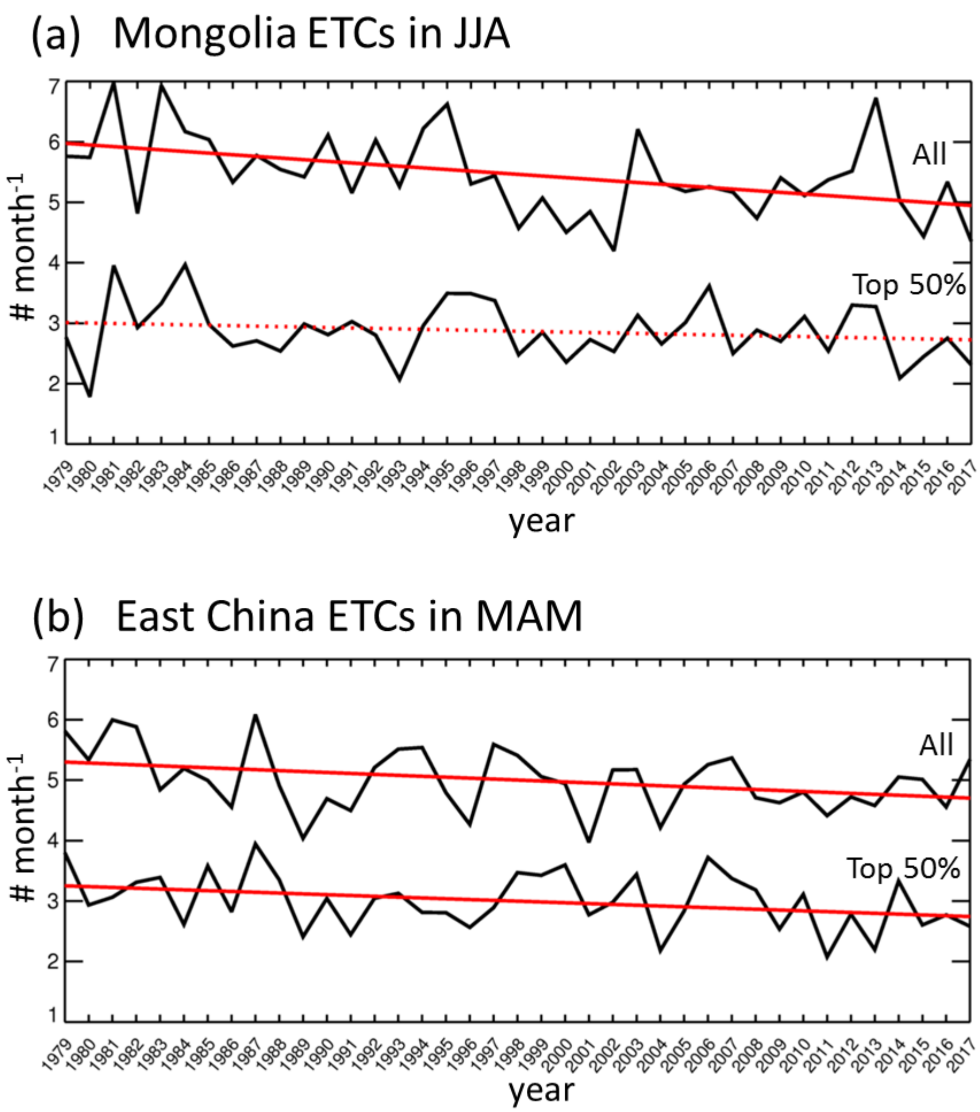

Fig. 9. Time series of ETC frequency and its linear trend for (a) summertime Mongolia ETCs and (b) springtime East China ETCs over the period of 1979–2017. Top 50% ETCs in intensity are separately shown. The solid red lines indicate statistically significant trends at the 95% confidence level.

This is a post-peer-review, pre-copyedit version of an article published in Climate Dynamics. The final authenticated version is available online at: https://doi.org/10.1007/s00382-019-05048-w

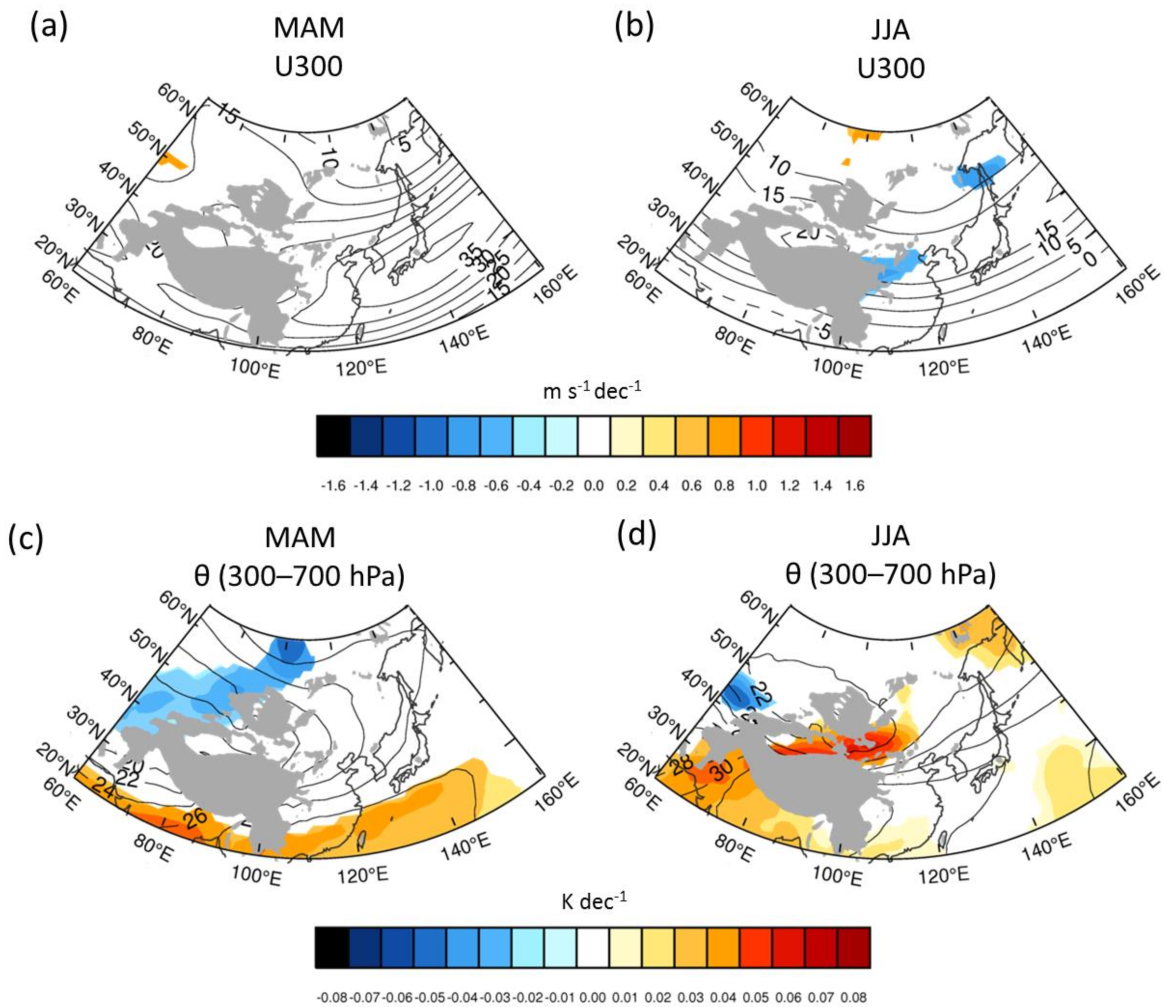

Fig. 10. Seasonal-mean (contours) and decadal trends (shaded) of 300-hPa zonal wind (top; in m s^{-1} dec^{-1}) and bulk static stability (bottom; in K dec^{-1}) in spring (left) and summer (right). Bulk static stability is defined by potential temperature difference between at the 300- and 700-hPa pressure levels. The trends that are statistically significant at the 95% confidence level are denoted with dots.

This is a post-peer-review, pre-copyedit version of an article published in Climate Dynamics. The final authenticated version is available online at: https://doi.org/10.1007/s00382-019-05048-w

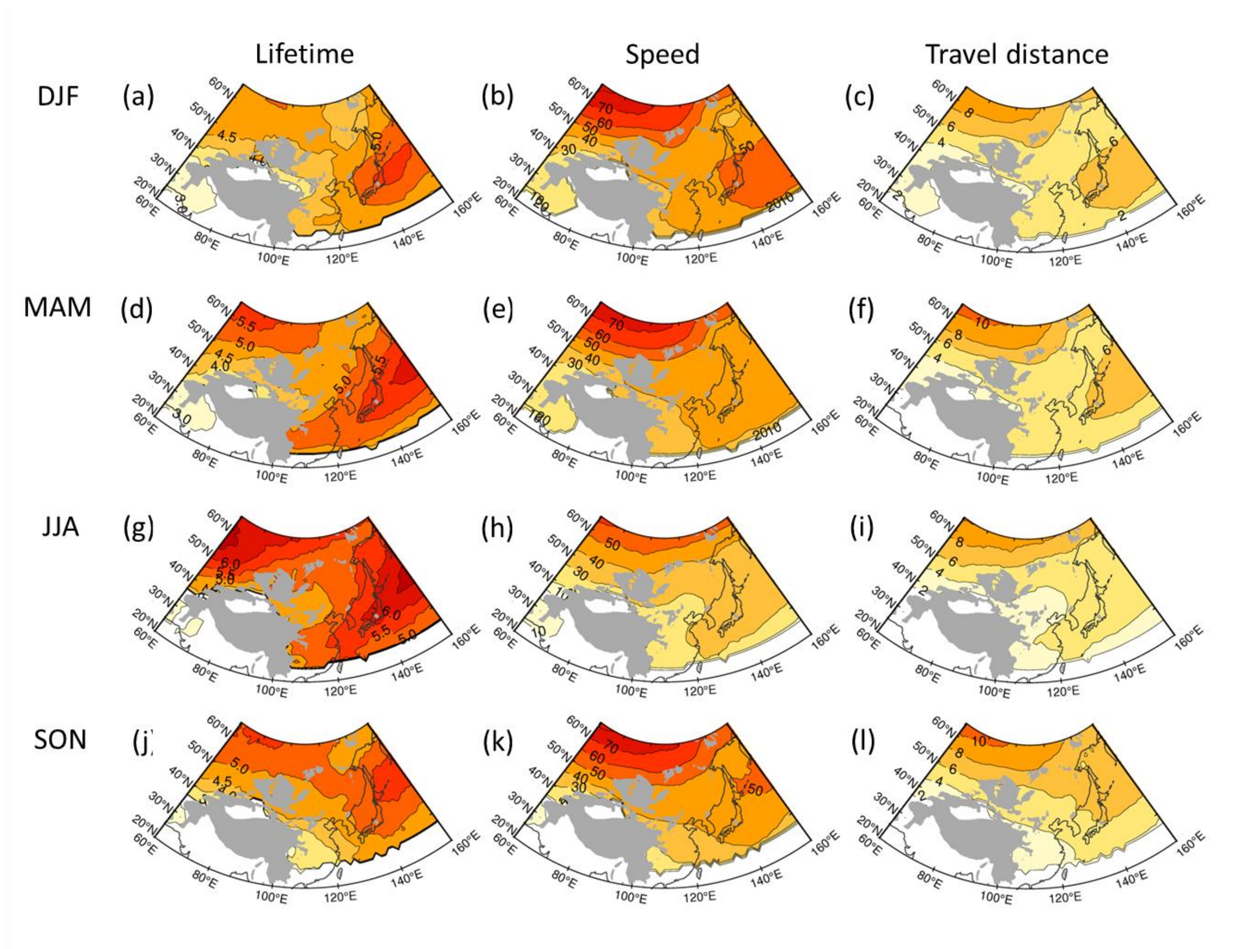

Fig. S1. Seasonal cycles of (left) lifetime (in day), (middle) speed (in km h^{-1}), and (right column) travel distance (in 10^3 km) of East Asian ETCs in (first) winter, (second) spring, (third) summer, and (fourth row) fall.